

InDiD: Instant Disorder Detection via Representation Learning

Evgenia Romanenkova
Skoltech
Russia, Moscow
shulgina@phystech.edu

Matvey Morozov
Skoltech
Russia, Moscow

Alexander Stepikin
Skoltech
Russia, Moscow

Alexey Zaysev
Skoltech
Russia, Moscow

Abstract

For sequential data, change points are moments of abrupt regime switches. Such changes appear in different scenarios, including complex video surveillance, and we need to detect them as fast as possible. Classic approaches for change point detection (CPD) perform poorly for semi-structured sequential data because of the absence of adequate data representation learning procedure. We propose a principled loss function that approximates classic rigorous solutions but is differentiable and makes possible representation learning. This loss function balances change detection delay and time to false alarm to provide a successful model for CPD. In experiments, we consider simple series and more complex real-world image sequences and videos with change points. For more complex problems, we show that we need more meaningful representations tailored for the specificity of the CPD task. Taking this into account, the proposed approach InDiD improves baseline results of CPD for various data types. For explosion detection, $F1$ score for our method is 0.54 compared to baseline scores 0.46 and 0.30.

1. Introduction

Modern industry uses complicated systems that continuously work online and are vital for the well-being of large companies and humankind in general. Collapses and prolonged unavailability of such systems lead to significant losses to business owners, so it's essential to detect deviations in their behaviour as fast as possible. A model trained on historical data on disorder detection deals with this problem and can signal distribution shifts online. Typically, data during training and inference come from a sequential stream represented as either multivariate vectors from sensors or semi-structured data like videos or image sequences [19, 22].

A more general anomaly detection in sequential data develops in machine learning and deep learning. It adopts

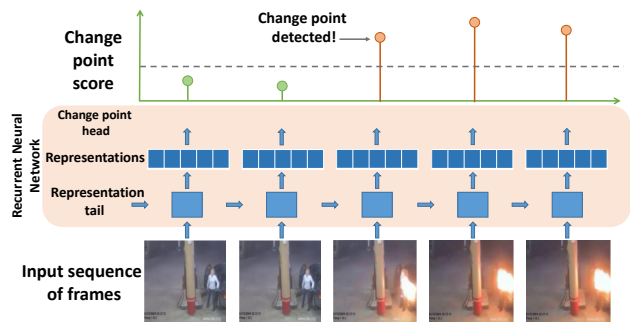


Figure 1. A scheme of work for representation-based change point detection approach

wide-spread methods and considers more specific models and loss functions [19]. However, the majority of existing methods concentrate on detecting an anomaly in a sequence instead of an accurate *anomaly moment* detection [13, 16]. An alternative approach comes from Change Point Detection (CPD) area: we aim to minimize the delay to disorder detection and the number of false alarms. The CPD problem statement better reflects industrial needs in various scenarios. While in need, examples of using modern deep learning techniques for CPD are scarce if the input data are semi-structured [1, 21].

One of the challenges here is that criteria related to the change detection delay and the number of false alarms are discontinuous and hard to compute. Thus, including them in a representation learning framework is not straightforward, making deep representation learning impossible. Another limitation when considering a CPD problem is a desire to work in an online mode, as it is the most reasonable and applicable for real-world problems [23]. Some simple ad-hoc approaches can be proposed to handle all these challenges. However, as they don't take into account the specifics of the problem, they often fail, especially if the amount of labeled data is small. So, we need a framework based on repre-

sensation learning to bridge the gap between industrial and scientific needs and theory related to change point detection [21]. We expect such an approach to provide a high-quality solution for the CPD problem with semi-structured data, advancing both understanding principles of representation learning for disorder detection and improving deep learning model quality in this area.

Our main claims are the following:

- We present an Instant Disorder Detection (InDID) framework for the change-point detection for semi-structured data. The method detects changes in the online mode and makes a decision based on the information available at the current moment in case of single and multiple change points to detect. The scheme of the framework is in Figure 1.
- To ensure fast and correct change detection, our loss function takes into account both task-specific criteria change point detection delay and a number of false alarms depicted in Figure 2. It approximates existing loss functions but is continuous and works directly with an intermediate deep learning model, allowing representation learning required for semi-structured data.
- Based on this loss function, we propose an end2end framework with a representation learning in the middle. This framework works with complex semi-structured data structures like multivariate data from sensors, series of images and videos. Our model is based on RNNs to handle the online nature of the problem and the need for a fast model and a typically small amount of available data.
- We conduct a thorough analysis of approach performance, including investigation of an embeddings space and various metrics for different datasets.

2. Related work

Change Point Detection is a widely studied problem in machine learning and statistics for sequential data. There are several approaches to state the problem. We follow the CPD problem statement that considers two natural performance measures for CPD: the detection delay and the number of false alarms [17]. Statistical methods based on likelihood like CUMSUM [14] and Posterior Probabilities statistics [20] are theoretically optimal for different combinations of this two performance measures [17]. These statistics accumulate during a run through a sequence: if a statistic exceeds a threshold, the model signals about a change point. As in many other cases, the theoretical optimality holds under quite strong assumptions or for simple input data.

Other methods aim to find an optimal partition of a signal [21, 22] to a part before and after the change point. For

this case, one can use methods based on searching through all possible partitions with or without regularisation terms in cost function [3, 11]. Although such methods have been known for a long time, they still are successful for different simple univariate time series [22] ahead of other more complex approaches like Kernel CPD [2, 7].

The comprehensive work [22] evaluated the most popular CPD methods on several sequences, included a small number of multivariate (with maximum dimension equals 4) and synthetic signals. The authors note that most recent methods perform poorly for multivariate sequences and require accurate hyperparameter selections. For a more in-depth overview with detailed descriptions of methods particularities and performances comparison, interested readers can look into review papers and books [1, 17, 21, 22].

Developing machine learning and deep learning methods allows considering more challenging scenarios with complex data that arise in practice. The most straightforward method to work with complex structures is to embed them into a low-dimensional space, where classic CPD methods are known to work. In the paper [15], authors propose to obtain low-dimensional representations using classic machine learning approaches. On top of it, they apply anomaly statistics similar to [17]. The authors conclude that to create an industry-ready solution, we need both a classifier for anomalous/normal data and a change point detector to precisely identify a boundary between classes. It is also tempting to adopt various neural networks solutions to the CPD problem. A straightforward approach [9] uses a similar idea as in CPD based on the probability density ratio but compare representations from neural networks. However, they focus on signals with a small number of features, and the maximum dimension is in sequences based on MNIST with 64 features.

More interesting is to learn special representation by taking into account the particularities of a task. The authors of the paper [19] propose a dataset with surveillance video and consider anomaly detection by using multiple instances learning for the dataset with labelling on the whole-video-level. The idea is to bring closer representations of normal frames and move apart ones of anomaly frames. Another approach from learning video representations area that appeared in the paper [5] is to learn the model to detect the fact of change/anomaly in the small video sub-sequence and then apply it for full video. The representation learning in this scenario is challenging, as we should take into account the context, but it seems to be the only way to get high-performing models [10]. While not considering a specific CPD problem statement, the authors of these papers aim at anomaly detection and use similar datasets. Their methods are interesting but can't be directly adopted to CPD and require a lot of data to work.

Thus, the current state of the art shows that it is possible

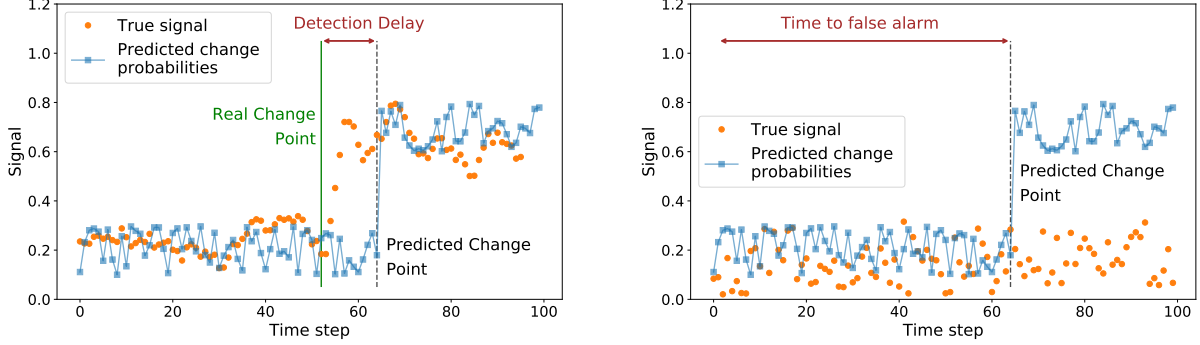


Figure 2. Examples of errors during change point detection: delayed change detection (left) and false alarm (right) and corresponding quality metrics Detection Delay and Time to False Alarm. Our approach minimizes a weighted sum of approximations of these loss functions.

to construct neural-networks based solutions for anomaly detection and learn corresponding representations. At the same time, they can't identify precise change moments crucial for many applications. On the other hand, a more theoretical area is related to change detection, but with too restrictive assumptions and limited ability to learn complex multivariate data representation. In our work, we tried to bridge this gap and proposed a principled solution for representation learning devoted to a change point detection problem. As the amount of available data in such a problem is moderate, we'll focus on neural networks architectures with smaller number parameters like LSTMs [8] and GRUs [4].

3. Methods

3.1. Change point detection problem statement

Let's $\mathbf{x}_t \in \mathbb{R}^D$ denote the observation for time steps $t \in \{1, \dots, T\}$, where T is the length of considered signal. The $\theta \in \{1, \dots, T, \infty\}$ defines a change point if for $t < \theta$ the data come from f_∞ , and for $t \geq \theta$ — from the distribution f_0 . We denote f_θ the joint data distribution under the assumption that the change occurs at the moment θ . Thus, f_∞ is called the normal distribution and f_0 — abnormal. The problem is the quickest detection of the true change moment θ using as small amount of data as possible among all approaches with the small number of false alarms.

Following [17], we look for an optimal change point that minimizes the expected detection delay $\mathbb{E}_\theta(\tau - \theta)^+$ among all procedures \mathfrak{M}_a such that the Average Time to False alarm larger than some value a . We take expectation \mathbb{E}_θ with respect to the distribution f_θ , $\tau \in \{1, \dots, \infty\}$ all possible change moments and $g(x)^+ = \max(g(x), 0)$. More formally, we are looking for an optimal change point

$\tau^* \in \{1, \dots, \infty\}$ such that:

$$\tau^* = \arg \inf_{\tau \in \mathfrak{M}_a} \mathbb{E}_\theta(\tau - \theta)^+, \quad (1)$$

$$\text{where } \mathfrak{M}_a = \{\tau : \mathbb{E}_\theta(\tau | \tau < \theta) \geq a\}. \quad (2)$$

Using the method of Lagrange multipliers with parameter c , we rewrite (1) as a single criterion that consists of two terms:

$$\tau^* = \arg \inf_{\tau} L(\tau), \quad (3)$$

$$\text{where } L(\tau) = \mathbb{E}_\theta(\tau - \theta)^+ - c\mathbb{E}_\theta(\tau | \tau < \theta).$$

We can't directly evaluate these expectations. Moreover, a straightforward approximation produces a discontinuous loss function with respect to the parameters of the model. Thus, we need a differentiable alternative that is easy and stable to calculate.

3.2. Loss function for InDiD approach

For simplicity, we consider a set of sequences $D = \{(X_1, \theta_1), \dots, (X_N, \theta_N)\}$ with similar length T , change point θ_i is in $\{1, \dots, T, \infty\}$. Each X_i is a sequence of multivariate observations $\{\mathbf{x}_{ij}\}_{j=1}^T$. A model $f_{\mathbf{W}}$ produces series of outputs $f_{\mathbf{W}}(X_i^{1:t}) = \{p_t^i\}_{t=1}^T$ based only on the information $X_i^{1:t} = \{\mathbf{x}_{ij}\}_{j=1}^t \subset X_i$ available up to the moment t . So, it works in the online mode and doesn't require any information from the future to conclude that a change has happened. We suppose that the probability p_t^i correspond to the probability of a change point in a sequence X_i at a specified time moment t . As these probabilities are the probabilities of change according to our model, they allow calculating the change moment τ . We either select a threshold and signal the change point if the probability exceeds the threshold or report a change point with the given probability. Our goal is to construct a model $f_{\mathbf{W}}$ that minimizes the criteria (3) for the change point detection procedure described above.

We suggested a new principled loss function based on the above criteria for training a neural network model $f_{\mathbf{W}}$:

$$\tilde{\mathcal{L}}(f_{\mathbf{W}}, D, c, \hat{T}) = \tilde{\mathcal{L}}_{delay}(f_{\mathbf{W}}, D, \hat{T}) + c\tilde{\mathcal{L}}_{FA}(f_{\mathbf{W}}, D). \quad (4)$$

It consists of two terms. The first term represents delay detection:

$$\tilde{\mathcal{L}}_{delay}(f_{\mathbf{W}}, D, \hat{T}) = \frac{1}{N} \sum_{i=1}^N \left(\sum_{t=\theta_i}^{\hat{T}} (t - \theta_i) p_t^i \cdot \prod_{k=\theta_i}^{t-1} (1 - p_k^i) + (\hat{T} + 1 - \theta_i) \prod_{k=\theta_i}^{\hat{T}} (1 - p_k^i) \right), \quad (5)$$

where $\hat{T} \leq T$ — some hyperparameter that restricts the size of a considered segment.

The second term approximates mean time to false alarm:

$$\tilde{\mathcal{L}}_{FA}(f_{\mathbf{W}}, D) = -\frac{1}{N} \sum_{i=1}^N \left(\sum_{t=0}^{\tilde{T}_i} t p_t^i \prod_{k=0}^{t-1} (1 - p_k^i) - (\tilde{T}_i + 1) \prod_{k=0}^{\tilde{T}_i} (1 - p_k^i) \right), \text{ where } \tilde{T}_i = \min(\theta_i, T). \quad (6)$$

Theorem 3.1. *The loss function $\tilde{\mathcal{L}}(f_{\mathbf{W}}, D, c, \hat{T})$ from (4) is a lower bound for a Lagrangian for $L(\tau)$ from criteria (3).*

The proof is given in Appendix. So, given the results above, our differentiable loss function is a lower bound for a principled loss function in (3). We expect that the proposed loss is an accurate approximation to the true one since the high terms in the sums are negligible.

To sum up, the idea of proposed **InDiD** approach is to update the neural network $f_{\mathbf{W}}$ parameters according to principled differentiable loss $\tilde{\mathcal{L}}(f_{\mathbf{W}}, D)$ (4). As we process inputs sequentially, hidden states for our architecture would be representations of the current sequence tailored for change point detection. To regularize our model, we start with parameters \mathbf{W} of a pretrained classifier that distinguishes observations before and after change points. So, we either train our CPD model from scratch using the proposed loss to get the pure *CPD* method, or train a classifier with binary cross-entropy loss and then fine-tune it with our loss to get *InDiD* method.

3.3. Baselines

To evaluate the proposed approach, we consider several baselines based on the classical method and based on different representation learning techniques.

As classical methods, we use *BinSeg*, *PELT* and *Kernel-CPD* from the *ruptures* package presented in the paper [21].

We apply these methods for simpler CPD problems without a need to learn complex representations up to our MNIST-based problem.

More advanced strategies are connected with representation learning via neural networks. The first technique is to formulate the CPD problem as a binary classification problem: we classify each moment as a moment before or after a change to get the change point probabilities p_i . To train a model that predicts these probabilities, we use the binary cross-entropy loss *BCE* for predictions and true labels. We can train a model to distinguish separate elements and then apply such model to the sequence element-wise (*BCE_simple*) or use a more powerful *seq2seq* model that looks at all available data (*BCE_seq2seq*).

4. Experiments

In this section, we demonstrate how our change-point detection approach works in real-data scenarios. The main results are given for all datasets. Due to space limitations, we demonstrate more specific findings only via one dataset; as for other datasets, results were almost similar in our experiments. The code is published online¹

4.1. Comparison details

We mostly select hyperparameters of classic CPD approaches by using a grid-search procedure for maximizing the Cover metric (see 4.3). For classic CPD approaches that could produce the deterministic amount of change points, we set the corresponding parameter to 1 as we concentrate on the data with one change point. For approaches *InDiD*, *CPD_seq2seq*, *BCE_seq2seq*, we train a neural network with the same selected architecture with no other changes. For *BCE_simple*, we use a different architecture, as it proceeds images separately. We adopt best practices from the literature for hyperparameters and architecture selection for different datasets and data types. Implementation details are given in Appendix.

4.2. Datasets

We use sequential data with various complexity: from multivariate data from sensors to video datasets. Detailed information on datasets and their preprocessing are given in Appendix.

Synthetic sequences. We start with two toy examples: 1D and 100D Gaussians with a change in the mean of the distribution and without it. We also generated a Synthetic 1D dataset with the number of change points ranging from 0 to 9 to check how different approaches perform in multiple change-point detection scenarios. Two examples are given in Figure 3.

¹The code and data labeling are available at <https://anonymous.open.science/r/InDiD>

Table 1. Main quality metrics for considered CPD approaches. \uparrow marks metrics we want to maximize, \downarrow marks metrics we want to minimize. Best values are highlighted with **bold** font, second best values are underlined.

Method	Mean Time to FA \uparrow	Mean DD \downarrow	AUC \downarrow	F1 \uparrow	Covering \uparrow to FA \uparrow
1D Synthetic data					
BinSeg	66.20	0.40	na	0.4536	0.7475
PELT	97.48	0.58	na	0.4574	<u>0.9836</u>
Kernel CPD	64.73	<u>0.51</u>	na	0.6425	<u>0.7426</u>
CPD seq2seq	<u>98.08</u>	0.64	512.418	0.9860	0.9934
BCE seq2seq	98.08	0.64	512.418	0.9860	0.9934
InDiD	98.76	1.63	<u>519.551</u>	<u>0.9789</u>	0.9829
100D Synthetic data					
BinSeg	62.94	0.28	na	0.4496	0.7218
PELT	96.95	<u>0.05</u>	na	0.4656	<u>0.9875</u>
Kernel CPD	63.95	0.01	na	0.6517	<u>0.7360</u>
CPD seq2seq	<u>97.73</u>	0.06	468.527	1	0.9990
BCE seq2seq	<u>97.73</u>	0.06	468.527	1	0.9990
InDiD (ours)	98.23	2.49	600.719	<u>0.9643</u>	0.9671
Human Activity Recognition					
BinSeg	9.04	1.35	na	0.7734	0.7781
PELT	10.05	1.04	na	0.5826	0.8279
Kernel CPD	9.17	0.87	na	0.8746	0.8493
CPD seq2seq	<u>11.27</u>	0.29	<u>45.219</u>	0.9920	<u>0.9927</u>
BCE seq2seq	<u>11.27</u>	0.29	<u>45.219</u>	0.9920	<u>0.9927</u>
InDiD (ours)	11.45	<u>0.43</u>	40.007	<u>0.9830</u>	0.9934
Sequences of MNIST images					
BinSeg	29.16	1.23	na	0.4416	0.7089
PELT	4.97	0.03	na	0.0198	0.3239
Kernel CPD	28.18	4.79	na	0.5075	0.6131
BCE simple	47.06	0.52	153.882	0.8186	0.9780
CPD seq2seq	44.89	0.40	187.607	0.7241	0.9691
BCE seq2seq	45.06	0.51	206.020	0.7511	0.9706
InDiD (ours)	<u>45.09</u>	<u>0.29</u>	<u>179.261</u>	<u>0.7647</u>	<u>0.9774</u>
Explosions					
BCE simple	11.20	0.44	<u>8.388</u>	0.3023	0.8484
CPD seq2seq	<u>14.23</u>	1.54	9.466	0.4048	0.8798
BCE seq2seq	14.95	1.81	8.546	<u>0.4667</u>	<u>0.8836</u>
InDiD (ours)	12.76	<u>0.64</u>	7.470	0.5472	0.8955
Road Accidents					
BCE simple	9.69	0.48	12.486	0.0417	0.7817
CPD seq2seq	14.64	<u>2.18</u>	13.257	0.1176	0.8299
BCE seq2seq	15.23	2.32	<u>12.770</u>	0.1860	0.8440
InDiD (ours)	<u>15.20</u>	2.31	12.896	<u>0.1647</u>	<u>0.8418</u>

Human Activity Dataset. As a dataset with numerical sequences, we use the USC-HAD dataset [24] with 12 types of human activity. We sample subsequences with changes in the type of human activity and without it. Each sequence consists of measurements of 561 features during 20 time ticks.

Sequences of MNIST images. We generate another

dataset on the base of MNIST [12] images. With a Conditional Variational Autoencoder (CVAE) [18] we construct sequences with and without change. Sequences with a change start and end with two images from similar classes that smoothly transform one into another. Sequences with a change start and end with two images from different classes. We generated a balanced dataset of 1000 sequences with

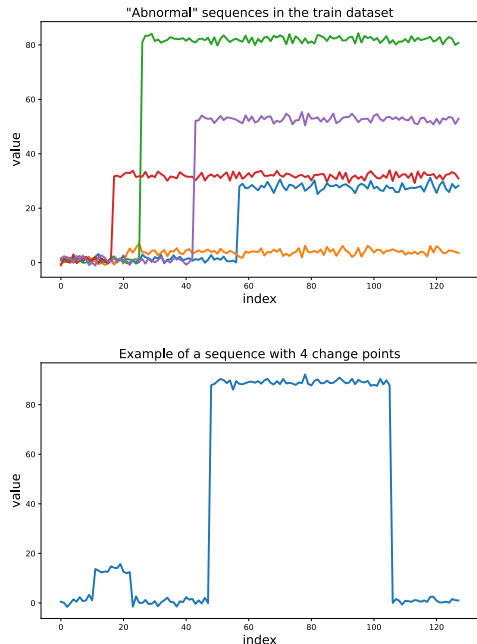


Figure 3. Examples of the generated 1D artificial sequences. Left: abnormal sequences from the training dataset; right: a sequence with 4 change points from the test dataset.

length 64.

Explosions and Car accidents. UCF-Crime is a video dataset for anomaly detection for sequences [19]. It consists of real-world 240x320 videos, with 13 realistic anomaly types such as explosions, road accidents, burglary, etc., and normal examples. We consider two types of anomalies: explosions and car accidents. *Explosions* correspond not to a point anomaly but to a distribution change. *Car accidents* follow a similar pattern but is a more challenging anomaly type, so we use it to test the limit of applicability of our approaches. We use samples from videos with a length of 16. We manually labeled frames related to the change point and provided this labeling along with our code.

4.3. Benchmarks and Metrics

Classification quality metrics. For our problem statement, elements of the confusion matrix have the following meaning. For True Positive (TP), we correctly detect changes no earlier than it appears. We report False Positive (FP) if a model predicts a change in a normal sequence or before an actual disorder. The True Negative (TN) indicates that we rightly don't detect anything. The False Negatives (FN) define cases when we don't detect the disorder while it appears in the real data. The most significant is the False Positive (FP). The obvious case of FP is predicting changes for normal signals. In addition, we detect the FP when the model predicts change before it appears in a sequence

with the real disorder. Based on these metrics, we calculate $F1_{our} = \frac{TP}{TP+0.5(FP+FN)}$. The F1 proposed in [22] doesn't penalize earlier detection, so we instead consider the definition above.

Delay detection and Time to False Alarm. For a quantitative comparison of CPD approaches, we concentrate on typical metrics for change point detection: Delay Detection and Time to False Alarm depicted in Figure 2. We want to meet two competing goals: minimize the Detection Delay and maximize the Time to False Alarm. The Delay Detection $(\tau - \theta)^+$ is the difference between the true change point θ and the model's prediction of change point τ . The Time to False Alarm τ is the difference between a first false positive prediction if it exists and the sequence start.

Area under the detection curve. We report as the change the first time when the model change probability prediction p_t exceed a threshold s . Varying s , we obtain different trade-offs between mean detection delay and mean time to a false alarm. To overview all possible options, we propose to measure the area under the curve obtained via varying the change detection threshold s . We want to find an approach that minimizes the area under such curve for x -axis Mean Time to False Alarm and y -axis Mean Detection Delay time. As this metric provides an overall performance evaluation, we consider it as the main quality metric for comparing our approaches.

Covering metric As a field-specific metric for CPD, we also examine the Covering metric (Cover) presented in [22]. The cover follows evaluation for the image segmentation problem, i.e. estimates the similarity of sequence partitions based on the model's predicted partition G' and true one G , i.e. $Cover(G, G') = \frac{1}{T} \sum_{A \in G} |A| \max_{A' \in G'} \frac{|A \cap A'|}{|A \cup A'|}$. The higher is the Cover, the better is the performance. [!h]

4.4. Main results

Table 1 presents metrics for various datasets. We consider the most important metrics F1 and AUC, as well as other metrics. It can be seen that our proposed methods outperform the baseline in terms of Delay Detection and Time to False Alarms while having lower common classification metrics.

We continue with Figure 4 on how threshold selection affects quality metrics for considered change detection approaches. For 1D synthetic cases, the performances of all models are similar due to the simple structure of the data. Our principled loss function provides performance improvements over BCE loss.

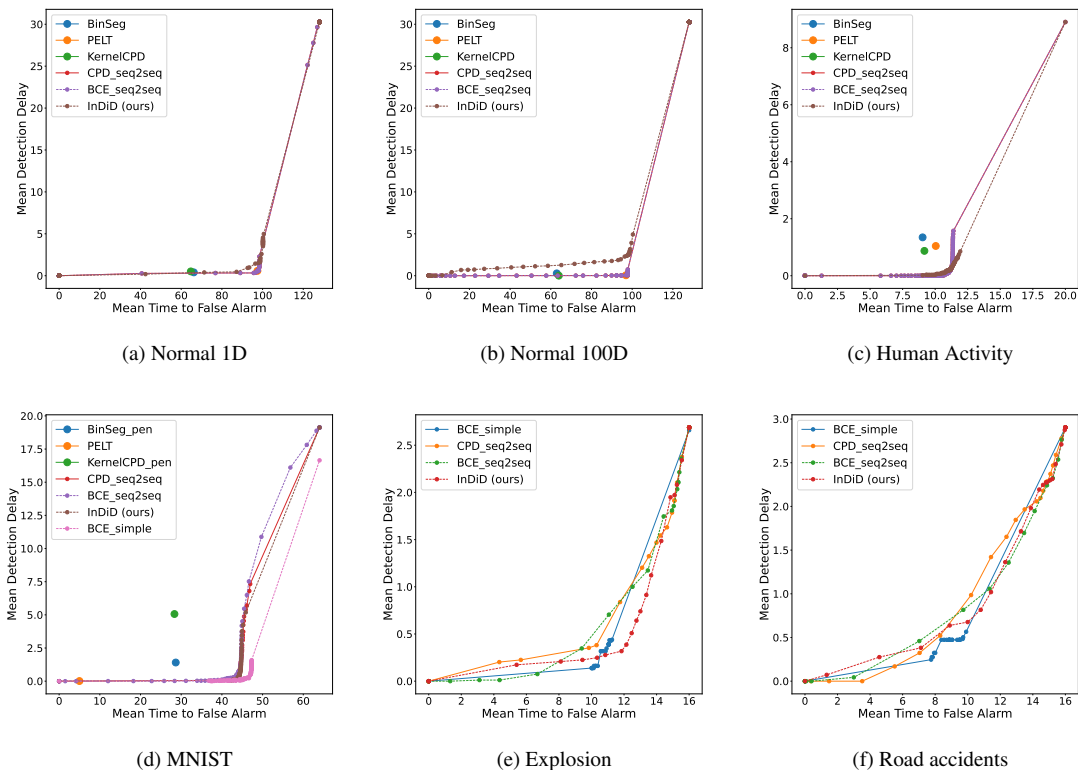


Figure 4. The performance detection curves for various datasets. If a method doesn't have a threshold to select, we plot a single point corresponding to its performance. The models trained with our losses have better results on all types of data except very simple cases, where performance is similar.

The results for 100D synthetic sequences and MNIST are ambiguous. Due to the simplicity of the problem, we have similar results for different approaches. But as we start to consider more structured data that requires heavier models to work, InDiD becomes better in terms of, e.g. F1 metric. For more complex data such as the Explosion video dataset, the InDiD model defeats the models with BCE loss. For Road Accidents data, we observe similar performances for all methods that construct representations. The main challenge for this method is the small amount of available data and complexity of change detection for such cases itself, as we see from low results F1 scores. InDiD keep almost top performance there too.

4.5. Score curves analysis

Figure 5 provides output model scores. It can be seen that models with BCE loss outputs probabilities are lower than our models with CPD or InDiD losses in a neighbourhood of a change point. For example, for the left picture in 5, the BCE model detects a change with a significant delay; for the left picture in 5, the BCE model has significantly higher scores without any actual change happening.

To check the quality of obtained representations, we

present tSNE embeddings for them in Figure 6. We show embeddings for MNIST data before, immediately after a change occurs and later. The model trained with BCE loss doesn't bother about fast change. Embeddings for points immediately after the change are close to that before the change. Thus, we'll have a significant detection delay. For our loss, embeddings for figures after change rapidly move to a separate region, making change point detection faster and more accurate. For the InDiD model, the embeddings after change lie even further with lower mixing of points before and after a change. Usage of InDiD improves representations in such areas compared to simpler BCE and CPD approaches.

4.6. Ablation study

Number of terms in loss We consider how many terms do we need to obtain a reasonable approximation that leads to a good model. As we see in Figure 7, our approximation is pretty accurate, and we don't need a large number of components in it. On the other hand, the inclusion of a larger number of components doesn't harm the numerical stability of our approach.

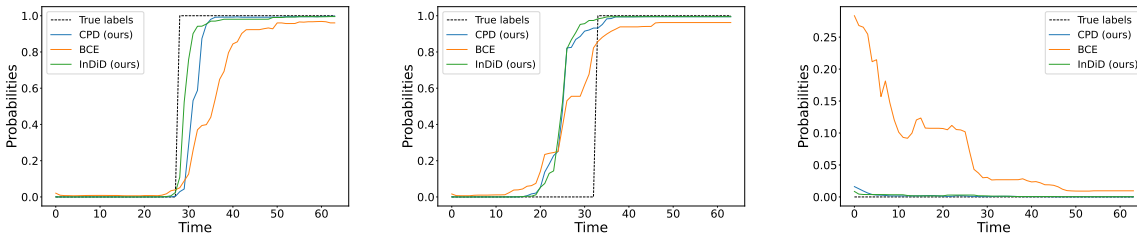


Figure 5. Typical examples with change point (left, center) and without (right) of model predictions for MNIST dataset.

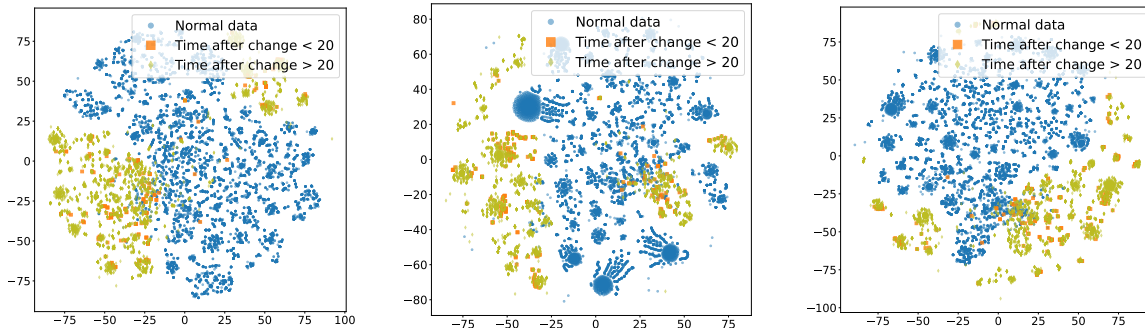


Figure 6. tSNE for embeddings obtained via approaches with the binary cross-entropy loss (left), our CPD loss (center), and combined InDiD approach (right).

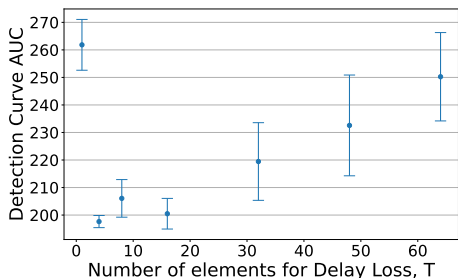


Figure 7. The model’s performance dependence on the number of elements for Delay Loss for MNIST data for InDiD averaged over 3 runs. We obtain reasonable and stable results if we include up to 20 or terms in our loss. For a larger number of terms, we see some degradation related to numerical issues.

Multiple CPD We investigated the performance of the considered models on synthetic 1-dimensional datasets with multiple change-points. We train various models on the Synthetic 1D with one change in the distribution and then apply the model to data with multiple disorders.

A deep model with our principled CPD loss outperforms the same model with BCE loss and common CPD baselines on both single- and multiple-change points synthetic datasets.

Method	Covering \uparrow
BinSeg	0.9187
KernelCPD	0.9536
BCE seq2seq	0.9533
InDiD (ours)	0.9891

Table 2. Metrics of CPD quality evaluated on a synthetic 1D multiple-changes dataset. The \uparrow means that we maximize the metric, **bold** text corresponds to the best metric values.

5. Conclusions and limitations

We proposed a principled loss function that allows quick change detection with a low number of false alarms for semi-structured sequential data. Our loss function is a differentiable lower bound for a criteria from the fundamental CPD literature. Thus, it allows end2end training of neural networks models for representation learning and quality metrics at hand. Our approach provides benefits in various scenarios, including the processing of data from sensors and video streams.

While promising, existing approaches have some limitations that we want to address. There is a need for a reasonably large labeled dataset to train decent models, and usage of pretrained general-purpose representations partially solves this problem. Another problem is the instability of anomaly scores. We deal with this problem by adding a

separate fully-connected layer between the video-frame embedding block and the recurrent block. However, in applications, classic score smoothing methods can help to maintain the numerical stability of CPD models.

References

- [1] Samaneh Aminikhanghahi and Diane J Cook. A survey of methods for time series change point detection. *Knowledge and information systems*, 51(2):339–367, 2017. 1, 2
- [2] Sylvain Arlot, Alain Celisse, and Zaid Harchaoui. A kernel multiple change-point algorithm via model selection. *Journal of machine learning research*, 20(162), 2019. 2
- [3] Jushan Bai. Estimating multiple breaks one at a time. *Econometric theory*, 13(3):315–352, 1997. 2
- [4] Kyunghyun Cho, Bart Van Merriënboer, Caglar Gulcehre, Dzmitry Bahdanau, Fethi Bougares, Holger Schwenk, and Yoshua Bengio. Learning phrase representations using rnn encoder-decoder for statistical machine translation. *arXiv preprint arXiv:1406.1078*, 2014. 3
- [5] Dave Epstein, Boyuan Chen, and Carl Vondrick. Oops! predicting unintentional action in video. In *Proceedings of the IEEE/CVF conference on computer vision and pattern recognition*, pages 919–929, 2020. 2
- [6] Christoph Feichtenhofer, Haoqi Fan, Jitendra Malik, and Kaiming He. Slowfast networks for video recognition. In *Proceedings of the IEEE/CVF international conference on computer vision*, pages 6202–6211, 2019. 12
- [7] Zaid Harchaoui, Eric Moulines, and Francis R Bach. Kernel change-point analysis. In *Advances in neural information processing systems*, pages 609–616, 2009. 2
- [8] Sepp Hochreiter and Jürgen Schmidhuber. Long short-term memory. *Neural computation*, 9(8):1735–1780, 1997. 3
- [9] Mikhail Hushchyn, Kenenbek Arzymatov, and Denis Derkach. Online neural networks for change-point detection. *arXiv preprint arXiv:2010.01388*, 2020. 2
- [10] Radu Tudor Ionescu, Fahad Shahbaz Khan, Mariana-Iuliana Georgescu, and Ling Shao. Object-centric auto-encoders and dummy anomalies for abnormal event detection in video. In *Proceedings of the IEEE/CVF Conference on Computer Vision and Pattern Recognition*, pages 7842–7851, 2019. 2
- [11] Rebecca Killick, Paul Fearnhead, and Idris A Eckley. Optimal detection of changepoints with a linear computational cost. *Journal of the American Statistical Association*, 107(500):1590–1598, 2012. 2
- [12] Yann LeCun and Corinna Cortes. MNIST handwritten digit database. 2010. 5
- [13] Dan Li, Dacheng Chen, Jonathan Goh, and See-kiong Ng. Anomaly detection with generative adversarial networks for multivariate time series. *arXiv preprint arXiv:1809.04758*, 2018. 1
- [14] Ewan S Page. Continuous inspection schemes. *Biometrika*, 41(1/2):100–115, 1954. 2
- [15] Evgeniya Romanenkova, Alexey Zaytsev, Nikita Klyuchnikov, Arseniy Gruzdev, Ksenia Antipova, Leyla Ismailova, Evgeny Burnaev, Artyom Semikhin, Vitaliy Koryabkin, Igor Simon, et al. Real-time data-driven detection of the rock-type alteration during a directional drilling. *IEEE Geoscience and Remote Sensing Letters*, 17(11):1861–1865, 2019. 2
- [16] Lifeng Shen, Zhuocong Li, and James Kwok. Timeseries anomaly detection using temporal hierarchical one-class network. *Advances in Neural Information Processing Systems*, 33:13016–13026, 2020. 1
- [17] AN Shiryaev. Stochastic change-point detection problems. *Moscow: MCCME (in Russian)*, 2017. 2, 3
- [18] Kihyuk Sohn, Honglak Lee, and Xinchen Yan. Learning structured output representation using deep conditional generative models. *Advances in neural information processing systems*, 28:3483–3491, 2015. 5, 11
- [19] Waqas Sultani, Chen Chen, and Mubarak Shah. Real-world anomaly detection in surveillance videos. In *Proceedings of the IEEE conference on computer vision and pattern recognition*, pages 6479–6488, 2018. 1, 2, 6, 11
- [20] Alexander G Tartakovsky and George V Moustakides. State-of-the-art in bayesian changepoint detection. *Sequential Analysis*, 29(2):125–145, 2010. 2
- [21] Charles Truong, Laurent Oudre, and Nicolas Vayatis. Selective review of offline change point detection methods. *Signal Processing*, 167:107299, 2020. 1, 2, 4
- [22] Gerrit JJ van den Burg and Christopher KI Williams. An evaluation of change point detection algorithms. *arXiv preprint arXiv:2003.06222*, 2020. 1, 2, 6
- [23] Mingze Xu, Mingfei Gao, Yi-Ting Chen, Larry S Davis, and David J Crandall. Temporal recurrent networks for online action detection. In *Proceedings of the IEEE/CVF International Conference on Computer Vision*, pages 5532–5541, 2019. 1
- [24] Mi Zhang and Alexander A Sawchuk. USC-HAD: a daily activity dataset for ubiquitous activity recognition using wearable sensors. In *Proceedings of the 2012 ACM Conference on Ubiquitous Computing*, pages 1036–1043, 2012. 5

A. Appendix

The supplementary materials contain proofs of suggested theorems in Section A.1, results on unbalanced dataset A.2, additional ablation studies in A.3, details about data preprocessing and data examples in Section A.4, implementation details in Section A.5.

A.1. Proofs

We provide proof that our loss function is a lower bound of the principled loss function. We start with two supplementary lemmas that lead to the main theorem.

Lemma A.1. $\tilde{\mathcal{L}}_{delay}(f_{\mathbf{w}}, D, \hat{T})$ is a lower bound for expected value of the detection delay.

Proof. The expected value of the detection delay \mathcal{L}_{delay} given the probabilities of a change point has the following form:

$$\begin{aligned} \mathcal{L}_{delay}(f_{\mathbf{w}}, D) &= \mathbb{E}_{\theta}(\tau - \theta)^+ = \\ &= \frac{1}{N} \sum_{i=1}^N \sum_{t=\theta_i}^{\infty} (t - \theta_i) p_t^i \prod_{k=\theta_i}^{t-1} (1 - p_k^i), \end{aligned}$$

the outer sum over i -s reflects that we average the loss over all sequences in a batch with change points at moments θ_i ; the inner sum over t -s correspond to losses associated with each moment in a sequence; p_t is the predicted probability of a change point at the moment t .

As it can be seen, the term includes an infinite number of elements. Moreover, their values decrease with each t . We rewrite $\mathcal{L}_{delay}(f_{\mathbf{w}}, D)$ in the following form for some T :

$$\begin{aligned} \mathcal{L}_{delay}(f_{\mathbf{w}}, D) &= \frac{1}{N} \sum_{i=1}^N \left(\sum_{t=\theta_i}^T (t - \theta_i) p_t^i \prod_{k=\theta_i}^{t-1} (1 - p_k^i) + \right. \\ &\quad \left. \sum_{t=T+1}^{\infty} (t - \theta_i) p_t^i \prod_{k=\theta_i}^{t-1} (1 - p_k^i) \right). \end{aligned}$$

Consider a lower bound for second term for a single sequence:

$$\sum_{t=T+1}^{\infty} (t - \theta) p_t \prod_{k=\theta}^{t-1} (1 - p_k) \geq (T + 1 - \theta) \sum_{t=T+1}^{\infty} p_t \prod_{k=\theta}^{t-1} (1 - p_k).$$

The expression under the sum introduces the probability of detecting the change moment after the moment $T + 1$. It equals to the probability of not detecting the change before moment $T + 1$. Thus,

$$(T + 1 - \theta) \sum_{t=T+1}^{\infty} p_t \prod_{k=\theta}^{t-1} (1 - p_k) = (T + 1 - \theta) \prod_{t=\theta}^T (1 - p_t).$$

This brings us to the desired result if we sum the first part and the lower bound for the second part. \square

Lemma A.2. $\tilde{\mathcal{L}}_{FA}(f_{\mathbf{w}}, D)$ is a lower bound for the expected value of the time to the false alarm.

The expected time to false alarm \mathcal{L}_{FA} given the probabilities has the following form:

$$\begin{aligned} \mathcal{L}_{FA}(f_{\mathbf{w}}, D) &= -\mathbb{E}_{\theta}(\tau | \tau < \theta) = \\ &= -\frac{1}{N} \sum_{i=1}^N \sum_{t=0}^{\theta_i} t p_t^i \prod_{k=0}^{t-1} (1 - p_k^i) \end{aligned} \quad (7)$$

The same situation with the infinite sum appears in (8) in case $\theta_i = \infty$ — when no change point happens. So, we offer an approximation for \mathcal{L}_{FA} :

$$\begin{aligned} \tilde{\mathcal{L}}_{FA}(f_{\mathbf{w}}, D) &= -\frac{1}{N} \sum_{i=1}^N \left(\sum_{t=0}^{\tilde{T}_i} t p_t^i \prod_{k=0}^{t-1} (1 - p_k^i) - \right. \\ &\quad \left. - (\tilde{T}_i + 1) \prod_{k=0}^{\tilde{T}_i} (1 - p_k^i) \right), \text{ where } \tilde{T}_i = \min(\theta_i, T). \end{aligned} \quad (8)$$

The proof is similar to the one from A.1.

Theorem A.1. The loss function $\tilde{\mathcal{L}}(f_{\mathbf{w}}, D, c, \hat{T})$ from (4) is a lower bound for $L(\tau)$ from criteria (3).

Proof. The proof follows from lemmas A.1 and A.2 as we provide a lower bound for both terms in the loss function in them. \square

A.2. Experiment on unbalanced dataset

In our main experiments, we mostly used balanced training datasets. They include an equal number of sequences with and without change-points. However, we expect to face change points less often than normal sequences without them in real-world data. Thus, to investigate the performance of proposed approaches in more realistic scenarios, we conduct additional experiments with sequences of MNIST images. We try a different number of sequences with change points and calculate the main quality metrics for them. As approaches to test, we consider different methods based on representation learning CPD seq2seq, BCE seq2seq, InDiD. The results are given in the Table 3.

We see that the performances of all the considered models deteriorate as the amount of "abnormal" data available for training decreases: Area under the Detection Curve increases, Covering decreases. However, the models are still able to detect change points quite precisely even in the scenario when the share of sequences with change points in the training dataset is less than 7%. Interestingly, the ranking according to different metrics changes: for a smaller number of sequences with changes, pure CPD seq2seq demonstrates better AUC and Covering values. At the same time, for the initial scenario, InDiD provides better quality.

# of seq. with CP	Model	AUC ↓	Covering ↑
350 (original)	CPD seq2seq	209.271 ± 15.946	0.9673 ± 0.0025
	BCE seq2seq	237.223 ± 4.188	0.9669 ± 0.0040
	InDiD	203.962 ± 18.543	0.9669 ± 0.0022
250	CPD seq2seq	224.732 ± 4.796	0.9671 ± 0.0029
	BCE seq2seq	241.308 ± 2.116	0.9654 ± 0.0038
	InDiD	224.524 ± 17.75	0.9665 ± 0.0031
150	CPD seq2seq	230.670 ± 5.569	0.9644 ± 0.0034
	BCE seq2seq	239.384 ± 3.802	0.9657 ± 0.0039
	InDiD	237.291 ± 16.594	0.9644 ± 0.0038
50	CPD seq2seq	237.782 ± 7.962	0.9618 ± 0.0058
	BCE seq2seq	245.962 ± 7.787	0.9616 ± 0.0046
	InDiD	247.354 ± 7.777	0.9621 ± 0.0046
25	CPD seq2seq	239.823 ± 11.628	0.9565 ± 0.0024
	BCE seq2seq	248.536 ± 5.652	0.9563 ± 0.0039
	InDiD	253.213 ± 13.437	0.9562 ± 0.0023

Table 3. Quality metrics for models trained on the datasets with smaller amount of sequences with change points (# of seq. with CP), while we use 350 sequences without change points for all experiments. The results are averaged by 3 runs and given in a format "mean ± std". **Bold** text highlights the best scores. ↑ sign marks the metrics we aim to maximize, ↓ - to minimize.

A.3. Ablation study

We conducted additional experiments to see if the training strategy affects the final model performance. Instead of training until one of the conditions is not fulfilled: loss no longer decreases or the maximum number of epochs achieved (see A.5), we train models used only Early stopping with patience 5. So, for some experiments optimal value exceeds the number of epochs for another scenario. The other details remain same.

Obtained performances for datasets Synthetic 1D, Synthetic 100D, Human Activity Recognition and Explosion are presented in Table 4 and in Figure 8. We don't add results for MNIST sequences and Road accidents as there is not a huge difference with the common training procedure. As we see, the InDiD approach shows a top or top two performance for all considered datasets in this scenario. We can argue that after enough training, our approach provides top performance.

A.4. Datasets details

In the paper, we consider a diverse set of datasets. Summary statistics on the data used are shown in Table 5. More information about data generation and preprocessing are provided below.

Synthetic datasets. The first part of a sequence in this dataset corresponded to the "normal" state and was sampled from $\mathcal{N}(1, 1)$ in a one-dimensional case or $\mathcal{N}(1, I)$ in a multi-dimensional case. As a change, we sampled vectors from a normal distribution with a uniformly randomly selected mean between 2 and 100 (constant vector for the

multivariate scenario) and the same variance as in the normal case.

Human Activity dataset contains sensors' records for 12 types of human physical activity, such as walking, elevator, going upstairs, running, sleeping, etc., collected from the group of 30 individuals. Each record has a length of 200 and consists of 561 features. The frequency of sensor measurements is 50 Hz. We cut these sequences so that there are sequences with changes in the type of human activity. The result length of every subsequence is 20.

Sequences of MNIST images. To generate data, we obtain a latent representation for MNIST images by using Conditional Variational Autoencoder [18] (CVAE). Then we take two points corresponding to a pair of digits and add the points from the line connecting two initial points. As a result, we have a sequence of latent representations of images. After reconstruction via CVAE's decoder, we get a sequence of images. Such approach allows us to generate images that change continuously, even if there is a change in a digit. There are sequences with (e.g. from 4 to 7) and without (e.g. from 4 to 4) a change point in the result dataset. We generate 1000 sequences with length 64 distributed evenly between normal and sequences with changes for our experiment. Two examples of obtained sequences are in Figure 9.

Explosions and Road Accidents. The whole dataset [19] consists of real-world 240×320 RGB videos, with 13 realistic anomaly types such as explosion, road accident, burglary, etc., and normal examples. As we've already mentioned, we use only explosion and road accident videos for our research. We assume that these types can be considered a change in distribution, while other types are point

Table 4. Main quality metrics for representation-based CPD approaches trained without maximum number of epochs’ restriction. \uparrow marks metrics we want to maximize, \downarrow marks metrics we want to minimize. Best values are highlighted with **bold** font, second best values are underlined.

Method	Mean Time to FA \uparrow	Mean DD \downarrow	AUC \downarrow	F1 \uparrow	Covering \uparrow
1D Synthetic data					
CPD seq2seq	94.45	0.48	595.961	0.9904	0.9952
BCE seq2seq	95.01	1.56	669.718	0.9839	0.9825
InDiD	<u>94.49</u>	<u>0.52</u>	<u>596.605</u>	0.9904	<u>0.9947</u>
100D Synthetic data					
CPD seq2seq	94.20	0.04	576.251	0.9968	0.9996
BCE seq2seq	94.29	0.13	<u>575.717</u>	0.9904	0.9998
InDiD (ours)	94.29	<u>0.05</u>	573.974	0.9968	0.9994
Human Activity Recognition					
CPD seq2seq	11.47	0.39	40.956	0.9843	0.9975
BCE seq2seq	10.92	0.19	51.807	0.9774	0.9653
InDiD (ours)	<u>11.35</u>	<u>0.36</u>	40.186	<u>0.9830</u>	<u>0.9929</u>
Explosions					
CPD seq2seq	15.22	2.03	10.396	0.3333	0.8607
BCE seq2seq	<u>14.61</u>	<u>1.51</u>	<u>6.971</u>	<u>0.4889</u>	<u>0.8963</u>
InDiD (ours)	14.18	0.92	6.423	0.6733	0.9295

anomalies. Given the small amount of data, we randomly chose a clip (a subsequence of whole frames’ sequences) from an abnormal subset for our research so that the explosion moment fell into the clip. For the normal subset, we pick clips randomly. Then, we generate sequences with the length 16 by sampling each 4th frame from these clips. The dataset was manually divided into training and validation sets, keeping the proportion of abnormal videos equal to 0.25 of which we are sampling 5 clips. The examples from the received data are shown in Figure 10.

A.5. Implementation details

Here we provide details on architectures and training for used datasets.

Synthetic datasets. We use an LSTM block with a hidden size of 4 in the case of 1D and 8 for 100D and dropout 0.5 followed by the output linear layer with sigmoid activation for experiments with synthetic datasets. We trained these networks till 50 epochs for BCE and CPD losses and used 50 epochs for the InDiD approach (epochs were equally distributed for BCE and CPD losses).

Human Activity dataset. We conduct our experiments with the Human Activity dataset using a model consisting of an LSTM block with 1 recurrent layers of 8 hidden dimensions. This block is followed by an output linear layer with the sigmoid activation. The maximum training epochs were set up to 50 in the case of CPD and BCE loss functions and 100 for the InDiD (epochs were equally distributed for BCE and CPD losses). The parameter T for CPD loss was set to 5.

Sequences of MNIST images. To generate sequences of MNIST images, we use CVAE with Encoder and Decoder consisting of linear layers. The hidden size was 256, and the latent dimension was 75. For main models on MNIST images, we use 1 layers LSTM with hidden size 32 followed by output layer with sigmoid activation functions. We train models maximally 100 epochs in all experiments. They were distributed equally for two losses for the InDiD approach. The parameter T for CPD loss was 32. As a baseline, we use a simple architecture that included 1 fully-connected layer with hidden size 50 followed by output layer with relu and dropout with $p = 0.5$. The maximum number of epochs was 20.

Video datasets. The architecture used in our experiments for video datasets consists of a CNN block and LSTM block. The CNN block includes all pre-trained features from 3D ResNet [6]. For explosion videos, we also apply 1-layer LSTM with a hidden size 16. After the RNN block, we use a linear layer with hidden size 32, ReLU and dropout with $p = 0.5$ and output layer. CPD and BCE models were trained till 20 epochs. For the InDiD approach, we use 10 epochs for each part. For road accident videos, we use 1-layer LSTM with hidden size 64 followed by output fully-connected layer with ReLU and dropout with $p = 0.5$. We have limited the maximum number of epochs for CPD and BCE with 100 epochs. For the InDiD approach, we use maximally 50 epochs for each part. The parameter T for CPD loss was set to 8 in both experiments.

For all experiments, we use the Adam optimizer with a learning rate of $1e^{-3}$ and early stopping with patience of 5.

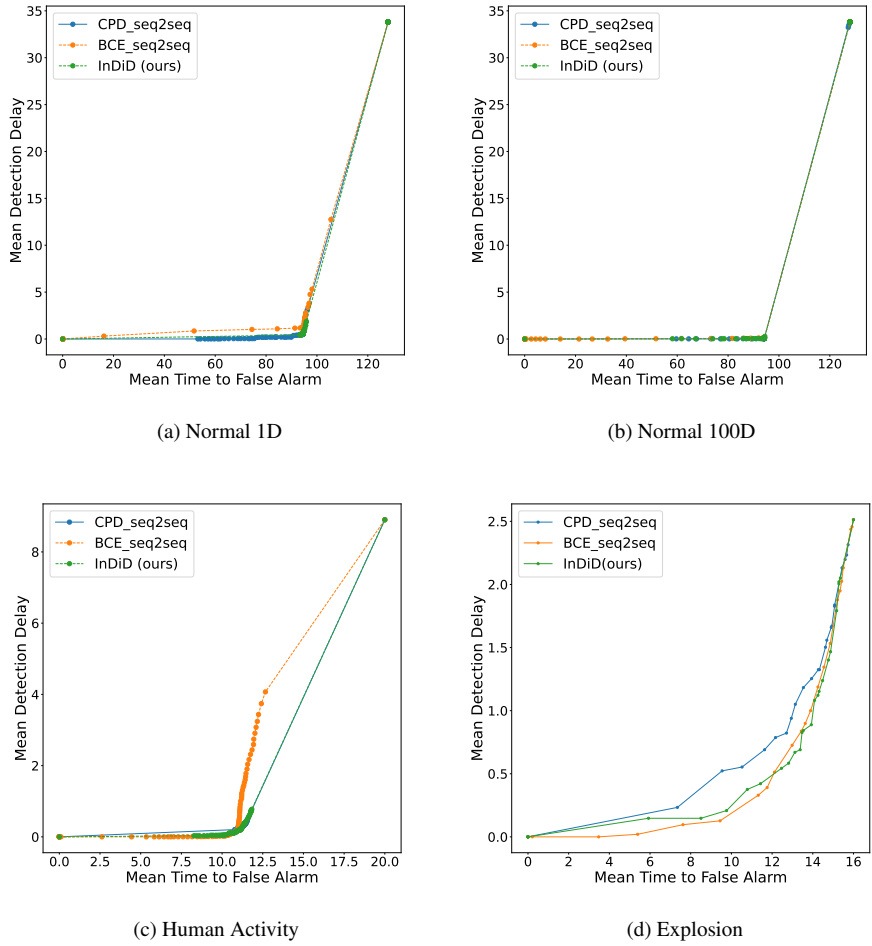


Figure 8. The performance detection curves for various datasets for training without epochs' restriction.

Table 5. Statistics for datasets used in our experiments.

Dataset	Single sample shape	Full dataset size	Test size	% of sequences with changes in test set	Sequence length
1D Normal	1×1	1000	300	52.7	128
100D Normal	100×1	1000	300	52.7	128
Human Activity	561×1	4917	1337	85	20
Seq.MNIST	$28 \times 28 \times 1$	700	300	47.3	64
Explosion	$320 \times 240 \times 3$	200	88	25	16

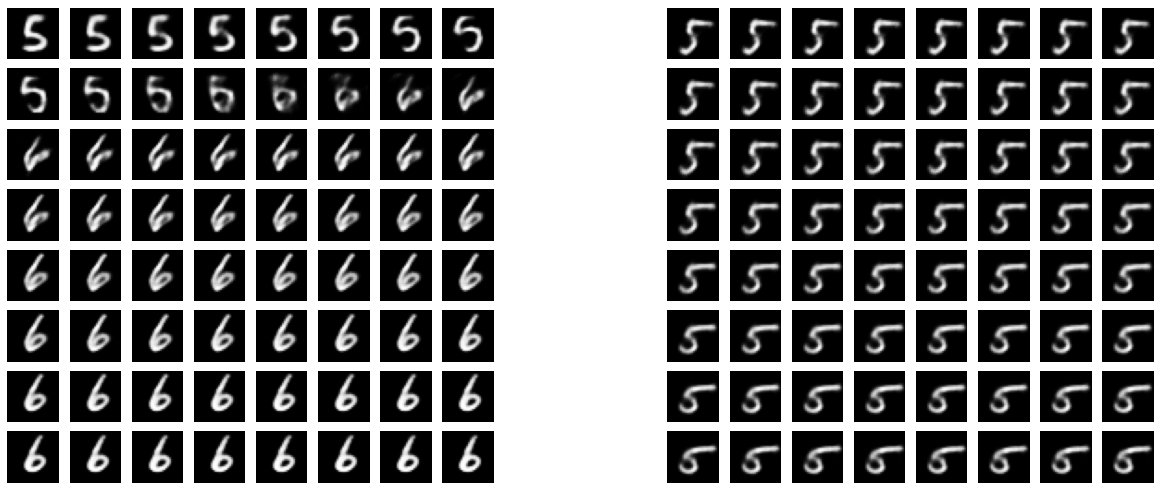


Figure 9. Example of MNIST sequences with (left) and without (right) change point. At each row a sequence goes from left to right. Then we continue with the leftest image in the next row.



Figure 10. Example from Explosion data with (left) and without (right) change point correspondingly. At each row a sequence goes from left to right. Then we continue with the leftest image in the next row.